Spontaneous network activity visualized by ultra-sensitive Ca^{2+} indicators, yellow cameleon-Nano

Kazuki Horikawa[1,2,*], Yoshiyuki Yamada[3,4,*], Tomoki Matsuda[1], Kentarou Kobayashi[1], Mitsuhiro Hashimoto[5], Toru Matsu-ura[4], Atsushi Miyawaki[6], Takayuki Michikawa[3,4], Katsuhiko Mikoshiba[3,4] and Takeharu Nagai[1,2,¶]

[1]Research Institute for Electronic Science, Hokkaido University, Kita-20, Nishi-10 Kita-ku, Sapporo, Hokkaido 001-0020, Japan

[2]Precursory Research for Embryonic Science, Japan Science and Technology Agency, Sanbancho, Chiyoda-ku, Tokyo 102-0075, Japan.

[3]Calcium Oscillation Project, Solution Oriented Research for Science and Technology, Japan Science and Technology Agency, Saitama 332-0012, Japan

[4]Laboratory for Developmental Neurobiology, RIKEN Brain Science Institute, Saitama 351-0198, Japan

[5]Hashimoto Research Unit, RIKEN Brain Science Institute, Saitama 351-0198, Japan

[6]Laboratory for Cell Function Dynamics, RIKEN Brain Science Institute, Saitama 351-0198, Japan

* Equal contribution

[¶]Correspondence should be addressed to T.N.

tnagai@es.hokudai.ac.jp

tel +81-11-706-9438

fax +81-11-706-9443

Abstract

We report a new set of ultra-sensitive Ca^{2+} indicators, yellow cameleon-Nano (YC-Nano), developed by engineering the Ca^{2+}-sensing domain of a genetically encoded Ca^{2+} indicator, YC2.60 or YC3.60. Their high Ca^{2+} affinities (K_d = 15-140 nM) and large signal change (1,450%) enabled detection of subtle Ca^{2+} transients associated with intercellular signaling dynamics and neuronal activity, even in 100,000-cell networks. These indicators will be useful for studying information processing in living multi-cellular networks.

To decipher the principles of information processing in multi-cellular networks, such as a brain or developing embryo, it is essential to record cellular activity with fine spatio-temporal resolution. Ca^{2+} imaging using synthetic or genetically encoded Ca^{2+} indicators (GECI)[1,2] is a particularly promising approach, because cells display a transient increase in intracellular Ca^{2+} concentration ($[Ca^{2+}]$) when they receive intercellular signals, as in synaptic transmission and hormonal stimulation. Cells have different $[Ca^{2+}]$s at rest and display $[Ca^{2+}]$ transients of different amplitudes ($\Delta[Ca^{2+}]$) upon stimulation that depend on the organism, cell type, and context of the stimulus. Therefore, optimizing the amount of Ca^{2+} indicator and its properties, including its Ca^{2+} affinity and Hill coefficient, is crucial for successful imaging.

In recent neuronal imaging, a synthetic Ca^{2+} indicator (Oregon green 488 BAPTA-1 (OGB-1); K_d = 170 nM)[1,3] or GECIs (D3cpV, TN-XXL , and GCaMP3)[4-6] are often used. All of them have a moderate Ca^{2+} affinity (K_d = 600-800 nM). In these reports, increasing the amount of Ca^{2+} indicator, e.g., by bolus loading of OGB-1 to a final concentration of 10-60 μM[3] or by expressing GECIs at 10 μM or more using a viral expression system[4], was necessary to improve the signal-to-noise ratio (SNR). However, it is not always possible to load large amounts of indicator: non-animal cells are often impermeable to indicators conjugated to acetoxymethyl esters[7,8], and general transgenic approaches result in low GECI expression levels[4]. Furthermore, some cells are estimated to have a very low resting $[Ca^{2+}]$ (for example, 30 nM for *Drosophila* larval presynaptic motoneuron boutons)[9] and display very small $\Delta[Ca^{2+}]$s, below the detection limit of low-affinity indicators, in response to action potentials.

An alternative way to detect subtle $[Ca^{2+}]$ changes at low concentrations (< 100 nM) is to utilize a small amount of a high-affinity indicator despite the poor SNR[10]. In

this case, it is crucial to choose an indicator with K_d that is in the middle of the [Ca^{2+}]s range to elicit the maximum changes in signal strength. However, only a limited number of high-affinity indicators (K_d < 100 nM; Quin2, D2cpV)[1,11] are available.

To overcome this problem, we sought to develop high-affinity indicators that would allow the sensitive detection of subtle [Ca^{2+}] changes. We derived our new indicators from a FRET-based Ca^{2+} indicator, yellow cameleon (YC) 2.60, which has a large dynamic range and relatively high affinity for Ca^{2+} (K_d = 95 nM, **Supplementary Table 1**, **Supplementary Note 1**)[12]. Even though YC2.60 has been successfully utilized for *in vivo* Ca^{2+} imaging[9], it is not always sensitive enough to detect the endogenous Ca^{2+} dynamics in living cellular networks (discussed below). The Ca^{2+} affinity of YC2.60 was previously modified by introducing mutations into the Ca^{2+}-binding pocket of the EF-hand motif in calmodulin (CaM) (E104Q and E31Q for YC3.60 and YC4.60, respectively); these modified indicators have a lower affinity than YC2.60, which contains wild-type CaM[12,13].

Here, we hypothesized that the flexibility of the linker peptide between CaM and the M13, a Ca^{2+}-CaM-binding peptide derived from myosin light chain kinase, would contribute to the Ca^{2+} affinity because a CaM-M13 fusion peptide connected with a longer linker (5-amino-acid with partially deleted M13) has a higher Ca^{2+} affinity (K_d = 18 nM)[14] than that with a shorter linker (Gly-Gly with intact M13; +2, K_d = 80nM)[15]. We therefore generated YCs with a longer linker, containing 3 to 8 amino acids (designated +3 to +8) (**Fig. 1a**). The Ca^{2+} affinity gradually increased as the linker was elongated and we named the resulting series of sensors, high-affinity yellow cameleons or "YC-Nano". For the +3 (Gly-Gly-Ser) linker the K_d was 50 nM (YC-Nano50) and for the +4 (Gly-Gly-Gly-Ser) linker the K_d was 30 nM (YC-Nano30). YCs with a +5 to +8

linker also had a higher affinity than YC2.60. The lowest K_d (= 15 nM) was achieved with a +5 linker (Gly-Gly-Gly-Gly-Ser) (YC-Nano15); this indicator had the highest affinity of any GECI reported so far[11] (**Fig. 1b**, **Supplementary Table 1** and **Supplementary Fig. 1**). Linker elongation was also effective for YC3.60, yielding YC-Nano140 (+4; Gly-Gly-Gly-Ser, K_d = 140 nM) and YC-Nano65 (+5; Gly-Gly-Gly-Gly-Ser, K_d = 65 nM) (**Fig. 1b**, **Supplementary Fig. 1** and **Supplementary Table 1**).

Kinetic measurement by stopped-flow fluorometry of YC-Nano140 and YC3.60 revealed that only the rate constant for the on reaction was increased, while that of the off reaction remained unchanged (**Supplementary Fig. 2**), suggesting that linker elongation accelerates the Ca^{2+}-induced conformational change of CaM-M13, which might be sterically restricted by the shorter linker (**Supplementary Note 2**). In spite of their increased Ca^{2+} affinity, these indicators maintained the large dynamic range (1,250–1,450%) of YC3.60 and 2.60 (**Supplementary Table 1**), which was achieved by an exceptionally high FRET efficiency (**Supplementary Fig. 3**).

To verify the advantages of YC-Nano for detecting subtle [Ca^{2+}] changes in living cells, we used the social amoeba *Dictyostelium discoideum* as an experimental platform. These cells exhibit Ca^{2+} transients when stimulated with a chemoattractant molecule, such as cAMP[7]. Because cAMP is also synthesized by the amoeba cells in the aggregation stage, we compared the range of [Ca^{2+}] change in response to both exogenous and endogenous stimuli. We obtained cells stably expressing YC2.60 or YC-Nano15 under the control of the Actin15 promoter. The morphology, growth rate, and developmental time-course of these cells were unaffected, suggesting that the

indicators were not toxic under these experimental conditions (**Supplementary Fig. 4**).

Stimulation with 10 μM cAMP yielded large FRET signal changes, assessed by ratiometric wide-field imaging of aggregation-competent cells (**Fig. 1c**). The YFP/CFP for the YC-Nano15- and YC2.60-expressing cells changed from 5.0 to 9.5 (ΔR = 4.5) and 2.0 to 6.2 (ΔR = 4.2), respectively. We next determined the amplitude of the Ca^{2+} transients associated with endogenous cAMP signaling, whose spatiotemporal pattern had never been directly visualized by conventional Ca^{2+} indicators. In response to stresses such as nutrient starvation, *Dictyostelium* cells start to aggregate by a cooperative self-organized process, in which propagating waves are established by the repeated synthesis and intercellular relay of cAMP at 6-10-min intervals. Under these conditions, YC-Nano15 showed a clear change in the FRET signal (ΔR = 2.5), whereas that of YC2.60 was almost undetectable (ΔR = 0.2) (**Fig. 1d** and **Supplementary Video 1**), indicating that YC-Nano15, unlike YC2.60, is quite useful to detect the small $\Delta[Ca^{2+}]$ in response to endogenous intercellular signals.

The increased signal strength achieved by optimizing the K_d also allowed us to perform Ca^{2+} imaging on a large spatial scale. The field of view for imaging could be expanded to a millimeter-sized network that included 100,000-*Dictyostelium* cells, in which the aggregation wave was clearly visible as a rotating spiral (**Supplementary Fig. 5**, **Supplementary Video 2,** ΔR_{Nano15} = 0.6), indicating that YC-Nano15, unlike YC2.60, was useful for detecting multi-cellular network activity in self-organized signaling dynamics ($\Delta R_{YC2.60}$ = 0.15, **Supplementary Fig. 6**, **Supplementary Video 3**).

We next tested the performance of YC-Nano in a neuronal system (**Supplementary Note 3 and Supplementary Figure 7**). For this, we examined YC-Nano's sensitivity for the subtle Ca^{2+} transient triggered by a single action potential (AP). YC-Nano15 and

YC3.60 cDNAs were introduced into mouse brain on embryonic day 14 using adenovirus vector and expressed under the control of the CAG promoter. Current pulses were injected into the soma of whole-cell-patched layer 2/3 pyramidal neurons (acute slices prepared on postnatal day 15-19 (P15-19)), and the FRET signal change at an apical dendrite was detected by two-photon microscopy. To correlate the number of APs and FRET signal changes, we elicited a series of current-triggered trains of 1, 2, 5, or 10 action potentials at a frequency of 20 Hz (**Fig. 2a**). For a single AP the maximal ratio change ($\Delta R/R_0$) in YC-Nano15 was almost double that in YC3.60, highlighting its increased sensitivity, but this decreased as the number of APs increased. This FRET signal change was also detected in the same acute-slice preparation from P72 mice, suggesting that YC-Nano15 could be chronically expressed without serious side effects under these experimental conditions (**Supplementary Fig. 7**). But YC-Nano15 is not suitable for the detection of the large Ca^{2+} transients triggered by high-frequency stimulus, due to the signal saturation and the slow decay time (3-4 sec) (**Fig. 2b,c**).

We further tested the performance of YC-Nano in the developing zebrafish embryo, which twitches spontaneously (**Supplementary Video 4**). We injected purified YC3.60 and YC-Nano50 proteins into fertilized eggs (**Fig. 3**, **Supplementary Note 4**), and measured the FRET signal change in neuron and muscle populations 20 hours later, using conventional confocal microscopy. In embryos loaded with YC3.60, we detected an almost identical baseline FRET signal (R_0 = 2.3) in all cell types (**Fig. 3**). In contrast, YC-Nano50 showed a high-to-low basal ratio in the epidermis, motor neurons, and fast/slow muscle, in this order, suggesting the possibility that these cells have different resting Ca^{2+} levels that cannot be differentially detected with a low-affinity indicator. Furthermore, in addition to the large FRET signal change in the motor neurons and fast

muscle detected by both YCs, only YC-Nano50 detected the subtle FRET signal change in slow muscle. This result demonstrated that the newly developed indicators are useful for detecting the spatio-temporal patterns of *in vivo* cellular activities, including subtle Ca^{2+} transients at low concentration ranges (**Supplementary Video 5**, **6** and **Supplementary Note 5**).

The YC-Nano series of ultra-sensitive Ca^{2+} indicators can detect the subtle Ca^{2+} transients associated with spontaneous network activity and reveal cell-type and stimulation dependent differences in both the resting Ca^{2+} level and the amplitude of Ca^{2+} transients. This indicates that the selection of indicators with the appropriate K_d is essential for successful *in vivo* Ca^{2+} imaging and a lineup of indicators with finely tuned K_d values optimized to detect [Ca^{2+}] from 10 nM to 100 nM would enable precise and reliable Ca^{2+} imaging, even in large-scale cellular networks.

Accession codes. GenBank, EMBL, Nucleotide Sequence Database and DNA Databank of Japan: GU071083, GU071084, GU071085, HM145948 and HM145949 (nucleotide sequence encoding YC-Nano15, YC-Nano30, YC-Nano50, YC-Nano65, and YC-Nano140, respectively).

Acknowledgments

We thank A. Nagasaki and Y. Kuramoto for instruction and assistance of the experiment using *Dictyostelium* cell. We also thank T. Kotani and S. Higashijima for assistance and instruction on fish embryo imaging. This work was partly supported by a Grant-in-Aid for Young Scientists (A) of the Japan Society for the Promotion of Science, and Scientific Research on Advanced Medical Technology of the Ministry of Labor, Health and Welfare of Japan to T.N., and a Grant from Precursory Research for Embryonic Science and Technology of the Japan Science and Technology Agency to T.N. and K.H.

Author contribution

K.H. and T.N. invented YC-Nano variants. Y.Y., M.H., A.M., T.Mi., and K.M. established the method of the expression of Ca^{2+} indicators in neurons using adenoviral vectors; K.H and T.M.. performed experiments other than electrophysiology and Ca^{2+} imaging in brain slices. K.H., T.Ma performed stopped-flow spectrometry. Y.Y. performed electrophysiology and Ca^{2+} imaging in brain slices; K.H., T.M., K.K., Y.Y., T.Ma., T.Mi. and T.N. analyzed data. K.H., Y.Y., T.Mi, and T.N. wrote the manuscript. T.N. supervised the study.

FIGURE LEGENDS

Figure 1 | Design and properties of the YC-Nano series of Ca^{2+} indicators. (**a**) Modified sequences of the peptide linker between CaM and M13. The CaM in YC3.60 and Nano140 has a mutation, E104Q. (**b**) Ca^{2+} titration curves for the indicators. The FRET signal change ($\Delta R/R_0$) is represented as a function of [Ca^{2+}] at 0-200 nM. n = 3; error bars, mean ± s.d. See also Supplementary Fig. 1. (**c, d**) Comparative Ca^{2+} measurement in *Dictyostelium discoideum*. Ca^{2+} transients detected with YC-Nano15 and YC2.60 in response to stimulation with 10 μM cAMP (gray bar) (c) or with endogenous cAMP during self-organized aggregation (d). See also Supplementary Video 1.

Figure 2 | Comparison of peak amplitude and time constant between YC3.60 and YC-Nano15 expressed in layer 2/3 pyramidal neurons in response to trains of action potentials. (**a**) Averaged peak amplitude ($\Delta R/R_0$) and (**b**) time constant for exponential decay (τ_{decay}) of the YC3.60 (black) and YC-Nano15 (red) responses are plotted against the number of action potentials. Error bars, mean ± s.d. (n = 5 for YC3.60 and n=7 for YC-Nano15). Data were collected from P15-P19 mice. (**c**) Response of YC3.60 or YC-Nano15 to the train of action potentials delivered at 0.5, 1, and 2 Hz. Bar, stimulus timing.

Figure 3 | Spontaneous motor activities in living zebrafish embryos. (**a, b**) Confocal images of embryos injected with YC-Nano50 or YC3.60 (YFP signal, horizontal view, right side is up and anterior to the left). Segmented muscles containing slow muscle

(sm) and fast muscles (fm) at the inner and outer side of the segment are located between the spinal cord and the epidermis (epi). The YFP/CFP ratio image (lower image) revealed high FRET signals for the subset of spinal neurons, fast muscles, and epidermis, and low FRET signals for the slow muscles, suggesting different basal Ca^{2+} levels among cell types. (**c, d**) Activity of motor neurons (MN), fast muscle (FM), and smooth muscle (SM) during the spontaneous twitching behavior detected with YC-Nano50 (c) and YC3.60 (d). Alternate firing on the right (upper panel) and left (lower panel) sides of the embryos was recorded at 2 Hz for 36 sec. Arrows and arrowheads indicate the timing of twitching. See also Supplementary Video 4 for the twitching behavior and Supplementary Video 5 for the FRET signal change. Scale bars, 50 μm.

METHODS

Gene construction. The peptide linker sequence between the CaM and M13 domains in YC2.60 and YC3.60 was replaced with -$(Gly)_n$-Ser-based flexible linkers, by PCR. For linkers composed of 3 to 5 amino acid residues, the cDNA of CaM was amplified with a GCATGC-tagged forward primer and -$(GGN)_{n-1}$-GGATCC-tagged reverse primer. The cDNA of M13-cp173Venus was amplified with a -GGATCC-tagged M13 forward primer and -GAATTC-tagged cp173 Venus reverse primer. After ligating the cDNA fragments of CaM and M13-cp173Venus at the *BamH*I site, the full-length cDNA of yellow cameleon was cloned into $pRSET_B$ (Invitrogen) by connecting a cDNA encoding ECFPΔ11 (cyan fluorescent protein with the C-terminal 11 amino acids deleted). To purify the recombinant proteins, strep tag II (IBA) was attached to the C-terminus of yellow cameleon, through an arginine-asparaginic acid linker.

Protein expression and purification. *E. coli* (JM109(DE3)) that was transformed with $pRSET_B$ (Invitrogen) containing the cDNA for yellow cameleons, was cultured for 60 hrs at 23°C with gentle shaking at 150 rpm. The recombinant proteins were sequentially purified by a Ni-NTA column (Qiagen) and StrepTactin beads (Qiagen), followed by gel filtration using a PD-10 column (GE Healthcare) to exchange the buffer with 5 mM HEPES, pH 7.2.

***In vitro* Ca^{2+} titration.** The emission spectra of the recombinant YC variants at 0.3 μM were measured by excitation at 430 nm using an F-2500 fluorescence spectrophotometer (Hitachi). Ca^{2+} titrations were performed by the reciprocal dilution of Ca^{2+}-saturated and Ca^{2+}-free buffers containing MOPS (10 mM), KCl (100 mM), and

EGTA (10 mM) or EDTA-OH (10 mM) with or without Ca^{2+} (10 mM) added as $CaCO_3$ at pH 7.2, room temperature[16]. The final concentration of free Ca^{2+} in reciprocally diluted solutions (24 solutions between 1.4 nM and 3 mM) was precisely determined individually using a Ca^{2+}-sensitive electrode (Metrohm)[17], which was calibrated with standard Ca^{2+} solutions purchased from Orion Research. The averaged data from three independent measurements was fitted to the Hill equation in a two-site model using Origin7 (OriginLab). To determine the FRET efficiency, 0.3 μM YC-Nano15 digested with proteinase K (final concentration 1 μg/mL) for 2 hours at 37 °C in the presence or absence of Ca^{2+} was also subjected to the spectrum measurement.

Kinetic measurement. Measurements of the Ca^{2+}-binding kinetics of YC were performed as described previously[13,18]. Briefly, a stopped-flow photometry system consisting of an RX.2000 rapid mixing stopped-flow unit (Leatherhead) and FP-750 spectrophotometer (JASCO) were used. The time course of the YFP emission change (excited with 430 nm) from Ca^{2+}-free to a pre-determined Ca^{2+} concentration was measured at 1,000 Hz. The time constants for the on reaction were calculated by performing curve fitting for a single exponential equation. The association and dissociation rate constants (k_{on} and k_{off}) were determined by fitting the data to the equation $k_{obs} = k_{on}\,[Ca^{2+}] + k_{off}$.

Culture and imaging of *Dictyostelium discoideum*. YC variants were expressed in Ax2 cells under the control of the Actin15 promoter. Briefly, the cells were electroporated with pBig expression vectors[19], and transformants were selected in HL5 medium containing 10 μg/mL G418 (Invitrogen). To initiate the self-organized aggregation, 10^8

cells were starved in development buffer (5 mM MES, 5 mM $CaCl_2$, 5 mM $MgCl_2$, pH 6.5) at 10^7 cells/ml. For smaller scale observation, aggregation-competent cells suspended in development buffer were plated on a glass-bottom dish (10^5 cell/cm^2) and imaged with a wide-field epifluorescence inverted microscope (TE2000, Nikon) equipped with 10x objectives (PlanApo, N.A. 0.45; Nikon). The samples were illuminated with a 100 W mercury arc-lamp through 6.25% and 12.5% neutral density filters, and a 438/20 excitation filter (Semrock). The fluorescence signals were split into two channels using the W-view system (Hamamatsu) to detect the donor CFP and acceptor YFP signals simultaneously through 480AF30 and 535DF25 interference filters (Omega), respectively, using an EM-CCD camera (ImagEM, Hamamatsu), every 3 seconds. For the large-scale observations, starved cells (2.5 x 10^6 cell/cm^2) were plated on a glass-bottom dish covered with a thin agarose layer and were imaged with 4x objectives (PlanApo, N.A. 0.2; Nikon). The CFP and YFP signals were sequentially captured every 15 seconds by using an emission filter changer (Ludl Electronic Products). The doubling time was determined for the suspension culture in 20 ml of HL5 containing G418 (10 μg/ml) shaken at 135 rpm.

Expression of YCs in neocortical layer 2/3 pyramidal neurons. YC3.60 and YC-Nano15 were introduced into layer 2/3 cortical pyramidal neurons by the *in utero* injection of recombinant adenovirus. The details of the procedures are described elsewhere (Yamada Y. et al., manuscript in preparation).. Briefly, YC3.60 and YC-Nano15 were subcloned into a cosmid vector carrying the CAG promoter (cytomegalovirus enhancer and β-actin promoter), woodchuck hepatitis virus post-transcriptional regulatory element, and bovine growth hormone polyadenylation

signal. The BspT104I-digested cosmid DNA was transfected into human embryonic kidney 293 cells (kindly provided by the Cell Resource Center for Biomedical Research, Institute of Development, Aging and Cancer, Tohoku University), and recombinant adenovirus was generated by the full-length DNA transfer method[20, 21]. Purified recombinant adenovirus was injected into the lateral ventricle of ICR mice on embryonic day 14.

Electrophysiology and Ca^{2+} imaging in acute brain slice

All experimental procedures were performed in accordance with the guidelines of the Animal Experiment Committee of the RIKEN Brain Science Institute. Mice were decapitated following ether anesthesia, and oblique parasagittal slices (300 μm) were prepared on postnatal day 15 or later, as described previously[22]. Whole-cell patch-clamp recording from the layer 2/3 pyramidal neurons was performed at 31-35°C. The patch pipettes were filled with the internal solution containing (mM): 140 K-gluconate, 4 NaCl, 10 HEPES, 4 Mg-ATP, 0.3 Na-GTP, 5 Na_2-phosphocreatine (pH 7.3 titrated with KOH, 285-295 mOsm). Slices were perfused at approximately 2 ml/min with artificial cerebral spinal fluid (ACSF) containing (mM): 125 NaCl, 2.5 KCl, 25 $NaHCO_3$, 25 $_D$-glucose, 1.25 NaH_2PO_4, 2 $CaCl_2$, 1 $MgCl_2$. ACSF was constantly bubbled with carbogen. Action potentials were elicited by brief somatic current pulses (1-3 nA, 2 ms). Electrophysiological signals were acquired with a MultiClamp 700B (Molecular Devices) and AxoGraphX software (AxoGraph Scientific).

CFP and YFP emission was acquired in line-scan mode (approximately 200 Hz) with a 2-photon laser-scanning microscope (FV300, Olympus) equipped with a 60x water immersion objective (LUMPlan Fl/IR NA 0.90, Olympus). A Ti:sapphire laser

(Maitai VF-TIM, Spectra-Physics) tuned to 840 nm was used for excitation. CFP and YFP signals were acquired with a dichroic mirror (510 nm, Chroma) and band-pass filters (480/40 nm and 535/30 nm for CFP and YFP, respectively, Chroma). The photomultiplier dark current was subtracted from all traces. The fractional change of the YFP/CFP emission ratio ($\Delta R/R_0$) was calculated. The mean baseline fluorescence ratio (R_0) was defined as the mean ratio of the approximately 1-second window immediately before the stimulus onset. The signal-to-noise ratio (SNR) was calculated as the peak amplitude divided by the baseline noise, where the peak amplitude was the maximum value of the $\Delta R/R_0$ trace filtered with a 35-ms moving window, and the baseline noise was the standard deviation of the raw trace during the baseline period, when R_0 was calculated. Statistical difference was assessed using a two-tailed Student's t-test ($p = 0.05$). Data analysis was performed with AxoGraphX, Igor Pro 6 (WaveMetrics), NeuroMatic (http://www.neuromatic.thinkrandom.com/), Fluoview (Olympus), ImageJ (NIH), and Excel (Microsoft) software.

Fish culture and imaging. *Danio rerio* obtained from a pet shop were kept under a 14/10-hr Light-Dark cycle, as described elsewhere[23]. The eggs were injected with purified protein (100 μM) to yield final cellular concentrations of around 5 μM, and allowed to develop at 28.5 °C. The concentration of loaded indicator was estimated from the emission intensity of YFP after excitation with a 515-nm laser line under confocal microscopy. For imaging, the embryos were mounted in a glass-bottom dish filled with 2% low-melting-point agarose. Ratiometric imaging was performed with a confocal microscope (A1, Nikon) equipped with water immersion 60x objectives (ApoVC, N.A. 1.20, Nikon). The samples were excited with a 458-nm multi-Argon ion

laser line, and images captured through emission filters (482/35 for CFP and 540/30 for YFP) were collected at 2 Hz.

REFERENCES

1. Paredes, R.M., Etzler, J.C., Watts, L.T., Zheng, W. & Lechleiter, J.D. *Methods* **46**, 143-151 (2008).

2. Kotlikoff, M.I. *J. Physiol.* **578**, 55-67 (2007).

3. Stosiek, C., Garaschuk, O., Holthoff, K. & Konnerth, A. *Proc. Natl. Acad. Sci. USA* **100**, 7319–7324 (2003).

4. Wallace, D.J. *et al*. *Nat*. *Methods*. **5**, 797-804 (2008).

5. Mank, M. *et al*. *Nat*. *Methods*. **5**, 805-811 (2008).

6. Tian, L. *et al*. *Nat*. *Methods*. **6**, 875-881 (2009).

7. Abe, T., Maeda, Y. & Iijima, T. *Differentiation*. **39**, 90-96 (1988).

8. Zhang, W.H., Rengel, Z. & Kuo, J. *Plant J*. **15**, 147-151 (1998).

9. Hendel, T. *et al. J. Neurosci.* **28**, 7399–7411 (2008).

10. Yasuda, R. *et al. Sci. STKE* **2004**, pl5 (2004).

11. Palmer, A.E. & Tsien, R.Y. *Nature Protoc.* **1**, 1057-1065 (2006).

12. Nagai, T., Yamada, S., Tominaga, T., Ichikawa, M. & Miyawaki, A. *Proc. Natl*. *Acad. Sci*. *USA* **101**, 10554-10559 (2004).

13. Miyawaki, A. *et al*. *Nature*. **388**, 882-887 (1997).

14. Martin, S.R. *et al*. *Biochemistry*. **35**, 3508-3517 (1996).

15. Porumb, T., Yau, P., Harvey, T.S. & Ikura, M. *Protein Eng*. **7,** 109-115 (1994).

16. Tsien, R.Y., Pozzan T. *Methods Enzymol.* **172** 230-262 (1989)

17. Bers, D.M. *Am. J. Physiol.* **242** C404–C408 (1982)

18. Matsu-ura, T. et al *J. Cell Biol.* **173** 755-65 (2006)

19. Nagasaki, A., de Hostos, E. L. & Uyeda, T. Q. P. *J. Cell Sci.* **115,** 2241-2251 (2001)

20. Mizuguchi, H., Kay, M. A. *Hum. Gene. Ther.* **9**(17)**:** 2577-2583 (1998)

21. Fukuda, H., Terashima, M., Koshikawa, M., Kanegae, Y., Saito, I. *Microbiol. Immunol.* **50**(8)**:** 643-654 (2006)

22. Davie, J.T. *et al. Nat. Protoc.* **1** 1235-1247 (2006)

23. Westerfield, M., The zebrafish book. A guide for the laboratory use of zebrafish (*Danio rerio*). 4th ed., (Univ. of Oregon Press, Eugene, 2000).

Horikawa et al., Figure 1

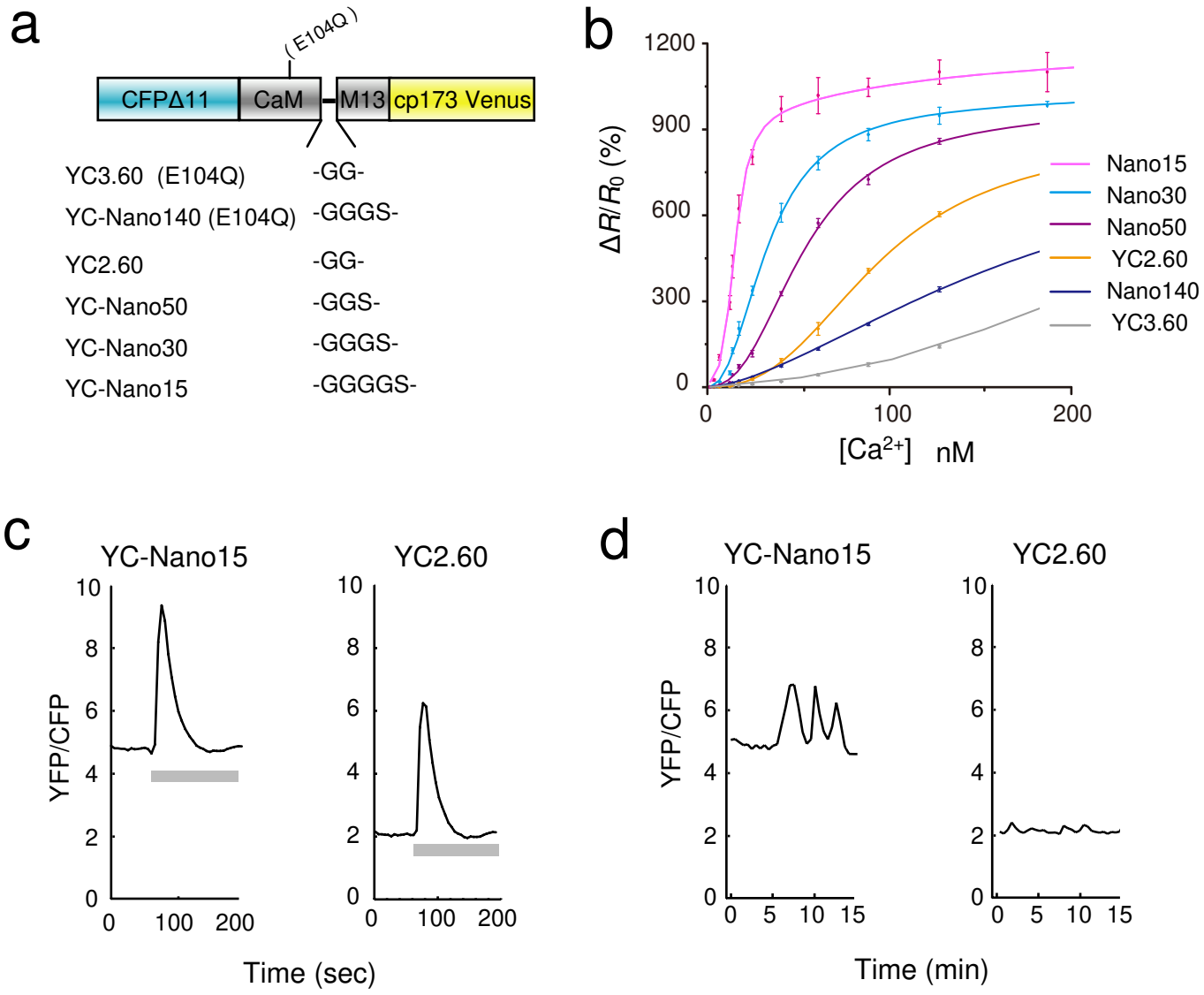

Horikawa et al., Figure 2

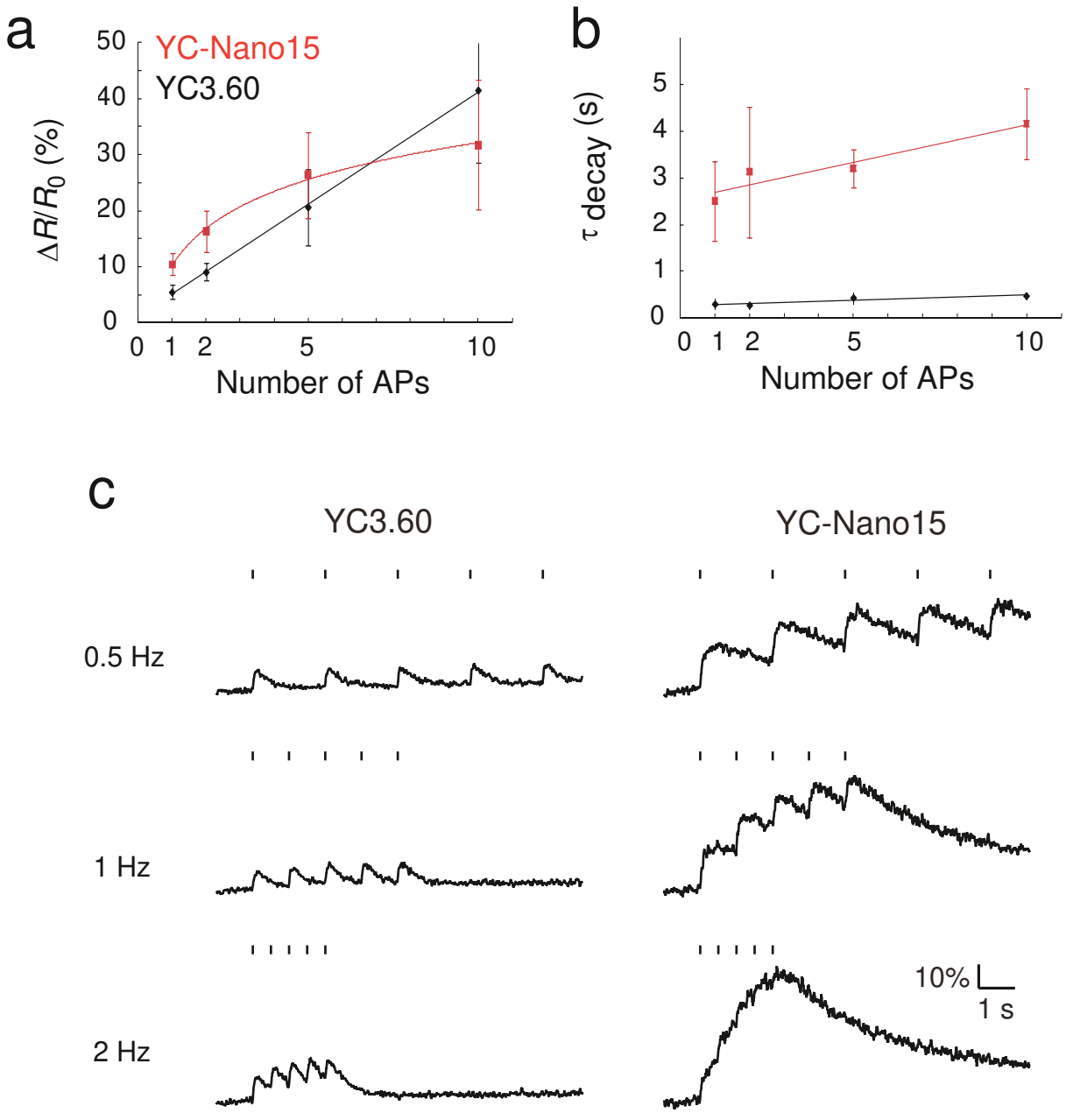

Horikawa et al., Figure 3

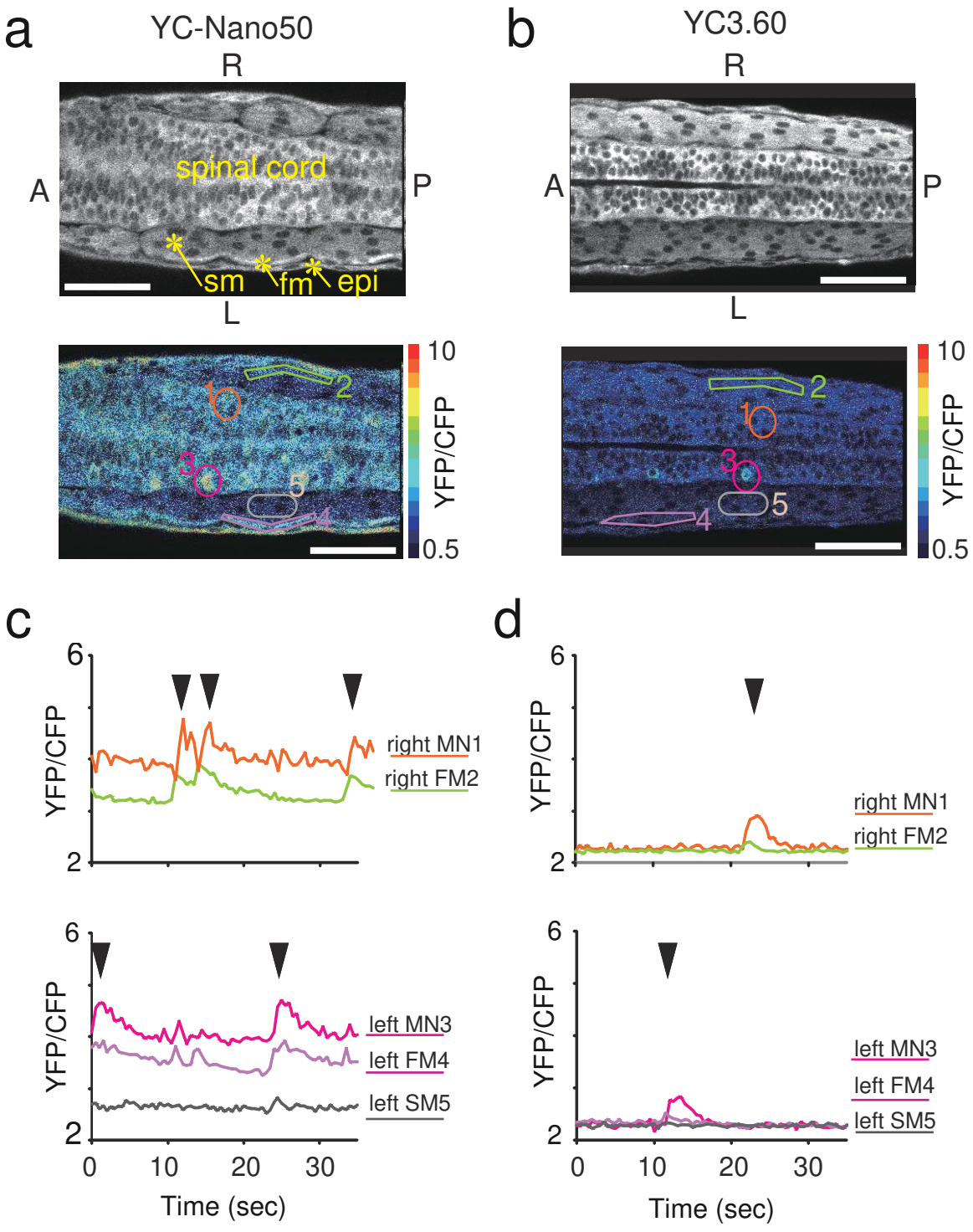

Supplementary File	Title
Supplementary Figure 1	Ca^{2+} affinity of the YC-Nano.
Supplementary Figure 2	Relaxation rate constant (k_{obs}) for YC3.60 or YC-Nano140 with Ca^{2+}.
Supplementary Figure 3	Spectra for YC-Nano15.
Supplementary Figure 4	Growth rate and developmental time course of *D. discoideum* cells expressing YC2.60 and YC-Nano15.
Supplementary Figure 5	Ca^{2+} imaging of spontaneous network activity in a 100,000-cell network.
Supplementary Figure 6	Aggregation waves of *Dictyostelium* cells visualized with YC2.60.
Supplementary Figure 7	YC3.60 and YC-Nano15 signals in response to trains of action potentials.
Supplementary Table 1	Properties of new YC variants
Supplementary Table 2	Electrophysiological properties of layer 2/3 pyramidal neurons expressing calcium sensors.
Supplementary Note 1	Biochemical properties of YCs
Supplementary Note 2	Kinetics analysis
Supplementary Note 3	Combined electrophysiology and two-photon imaging.
Supplementary Note 4	Toxicity of YC-Nano in short-term expression.
Supplementary Note5	Confocal imaging of the twitching behavior in zebrafish embryos.
Supplementary Video 1	Comparative visualization of Ca^{2+} dynamics in early aggregating stage of *Dictyostelium* cells visualized by YC-Nano15 and YC2.60
Supplementary Video 2	Ca^{2+} dynamics in aggregating *Dictyostelium* cells visualized by YC-Nano15
Supplementary Video 3	Ca^{2+} dynamics in aggregating *Dictyostelium* cells visualized by YC2.60
Supplementary Video 4	Twitching behaviour of zebrafish embryo
Supplementary Video 5S	Spontaneous motor activities in living zebrafish embryos visualized by YC-Nano50
Supplementary Video 6	Spontaneous motor activities in living zebrafish embryos visualized by YC3.60

AOP

Engineering of the Ca^{2+}-sensing domain in existing yellow cameleon Ca^{2+} indicators is used to create a series of indicators with a range of increased Ca^{2+} affinities capable of detecting subtle changes in intracellular Ca^{2+} at low resting levels.

ISSUE

Engineering of the Ca^{2+}-sensing domain in existing yellow cameleon Ca^{2+} indicators is used to create a series of indicators with a range of increased Ca^{2+} affinities capable of detecting subtle changes in intracellular Ca^{2+} at low resting levels.

Supplementary Figure 1 | Ca^{2+} affinity of the YC-Nano. The normalized FRET signal was plotted against the logarithmic representation of the Ca^{2+} concentration. Fitted curve for the averaged data of three independent measurements is presented. The YC2.60 and YC3.60 series are shown in the upper and lower panel, respectively.

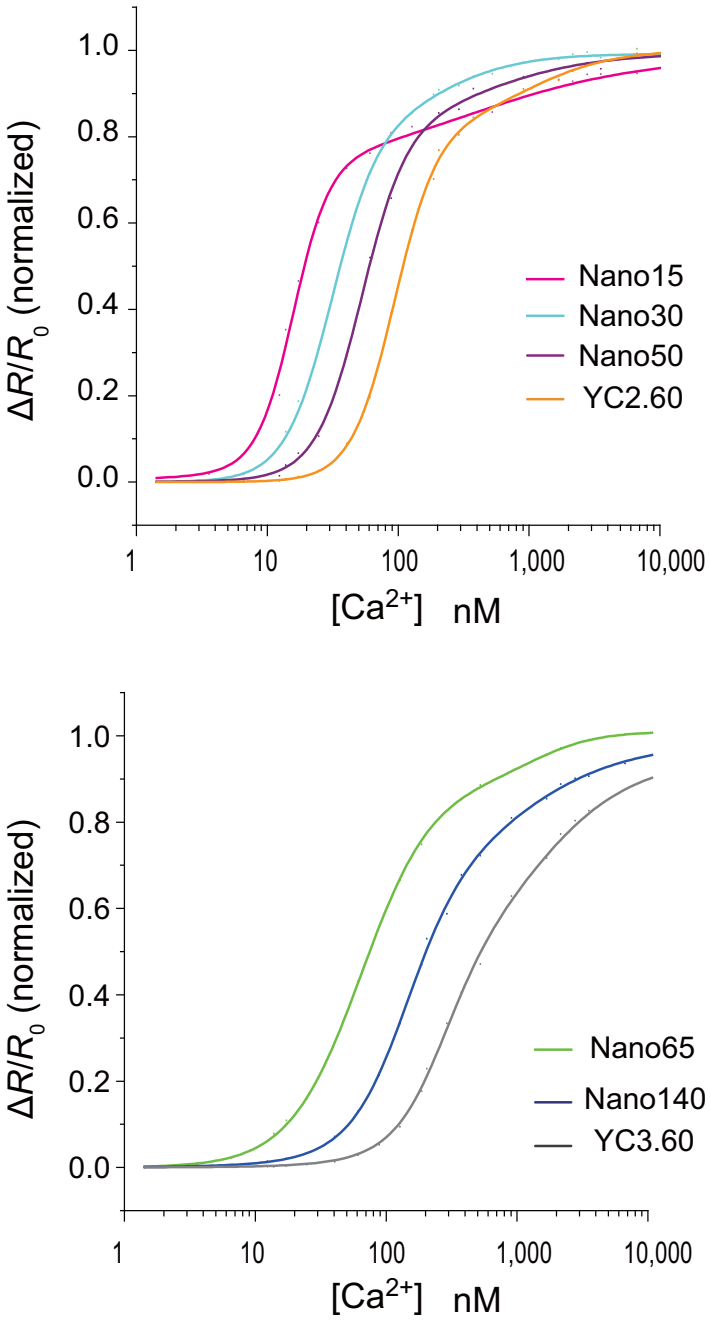

Supplementary Figure 2 | Relaxation rate constant (kobs) for YC3.60 or YC-Nano140 with Ca^{2+}. Association and dissociation rate constants (kon and koff) were determined by fitting to the equation $k_{obs} = k_{on}[Ca^{2+}] + k_{off}$. For details, see **Supplementary Note 2**.

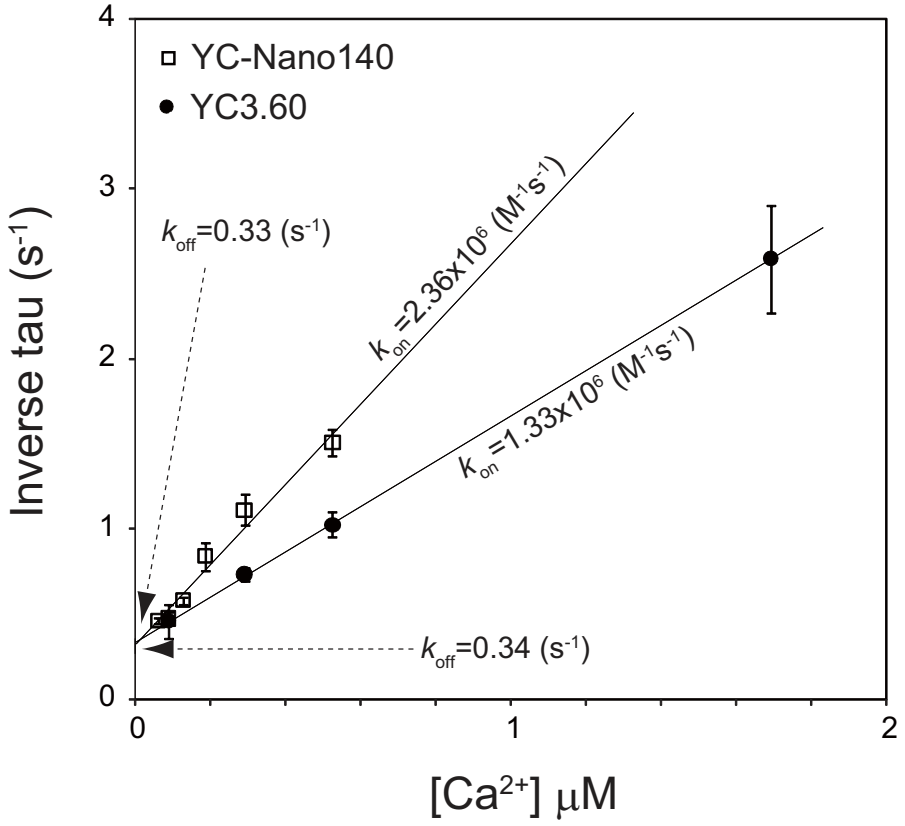

Supplementary Figure 3 | Spectra for YC-Nano15. Normalized fluorescent spectra of YC-Nano15 in the absence of Ca^{2+} (cyan) or in the presence of a saturating concentration of Ca^{2+} (magenta). The emission spectrum of proteinase K-digested YC-Nano15 is indicated in gray. For details, see **Supplementary Note 1.**

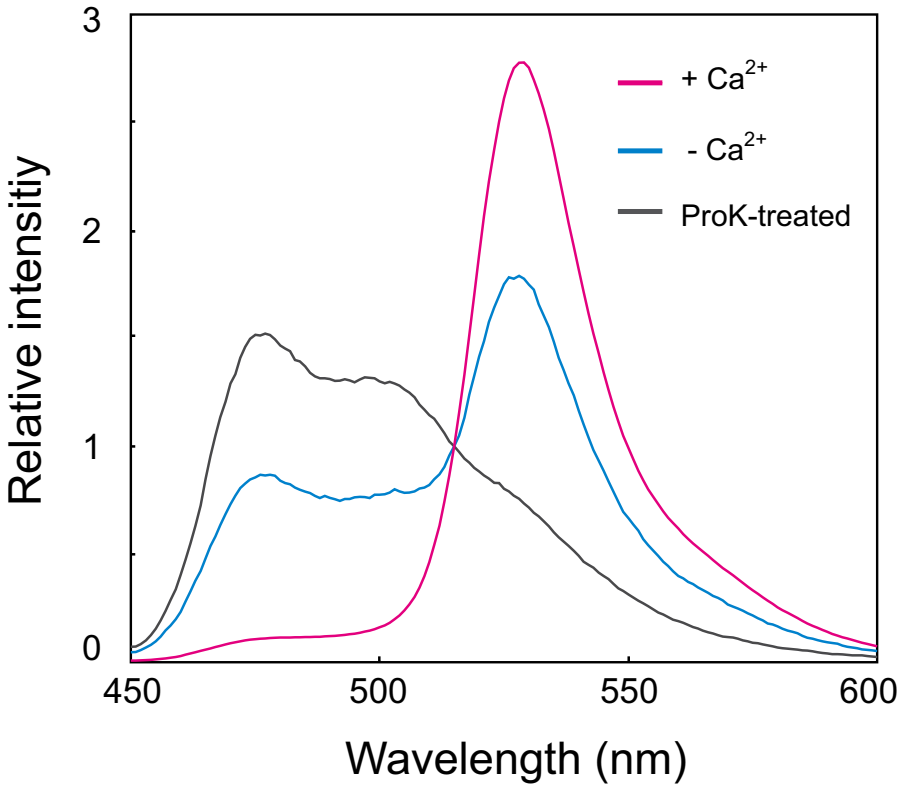

Supplementary Figure 4 | Growth rate and developmental time course of *D. discoideum* cells expressing YC2.60 and YC-Nano15. (**a-d**) Differential interference contrast images of cells before (**a, b**) and after (**c, d**) starvation. Note the rounded and elongated shapes characteristic of cells before and after starvation, respectively. (**e-j**) Development under semi-dry conditions. Aggregation stream (**e, f**) and low- (**g, h**) and high- (**i, j**) magnification views of the resulting fruiting bodies. (**k**) Doubling time of cells in the suspension culture.

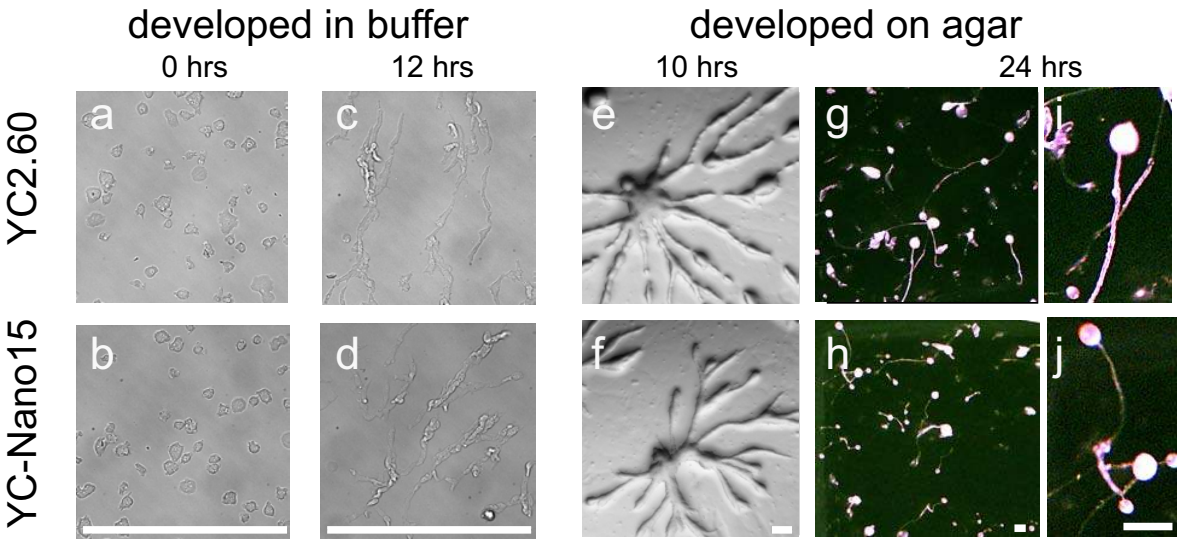

k

expressed gene	EGFP	YC2.60	YC-Nano15
doubling time (hrs)	8.1	8.3	8.1

Supplementary Figure 5 | Ca^{2+} imaging of spontaneous network activity in a 100,000-cell network. (a, b) Spiral-shaped intercellular signaling wave in a 100,000-cell network of *Dictyostelium discoideum* visualized by YC-Nano15. YFP (a) and YFP/CFP ratio images (b) in a 2 mm x 2 mm field of view. (c) The spatiotemporal wave pattern in the yellow inset of panel b is represented as a kymograph (every 15 seconds for 15 minutes). (d) Time course of the FRET signal change in the white box in b. See also Supplementary Video 2. Scale bar, 2 mm.

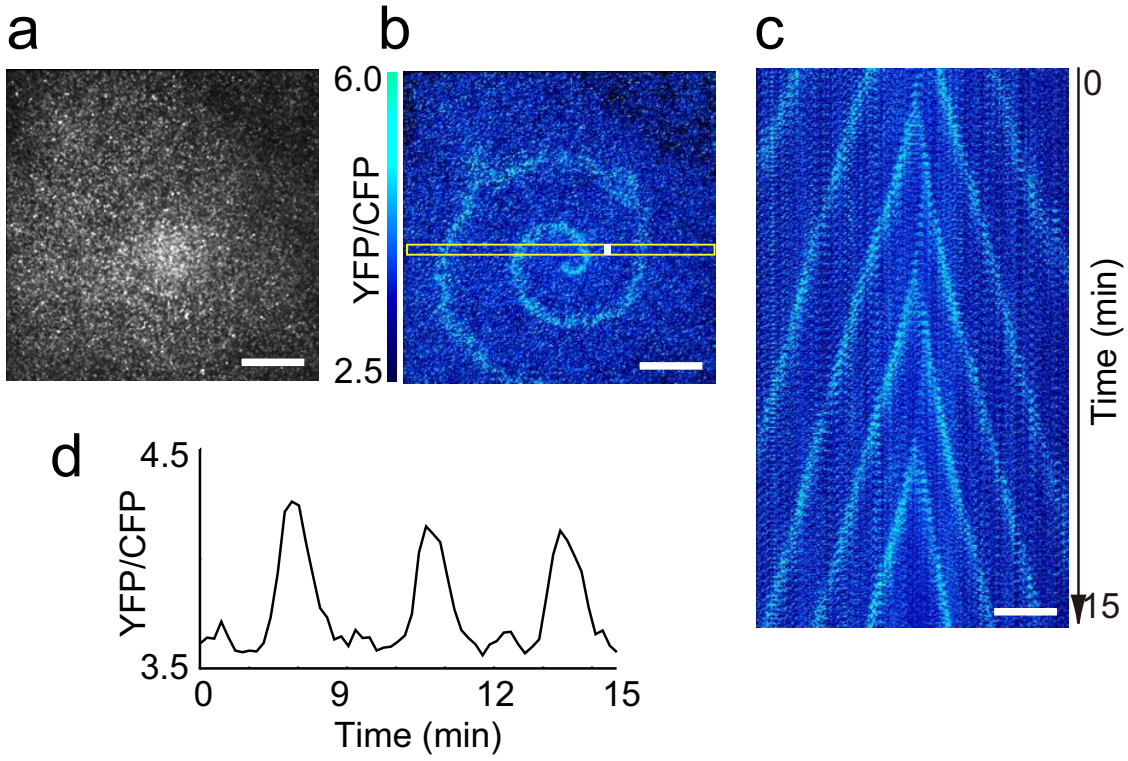

Supplementary Figure 6 | Aggregation waves of *Dictyostelium* cells visualized with YC2.60. (a, b) Spiral-shaped intercellular signaling wave in a 100,000-cell network of *Dictyostelium discoideum* visualized by YC2.60. a and b show YFP and YFP/CFP ratio images, respectively . (c) The spatiotemporal wave pattern in the yellow inset of panel b is represented as a kymograph (every 15 seconds for 15 minutes). (d) Time course of the FRET signal change in the white box in b. Scale bar, 1 mm..

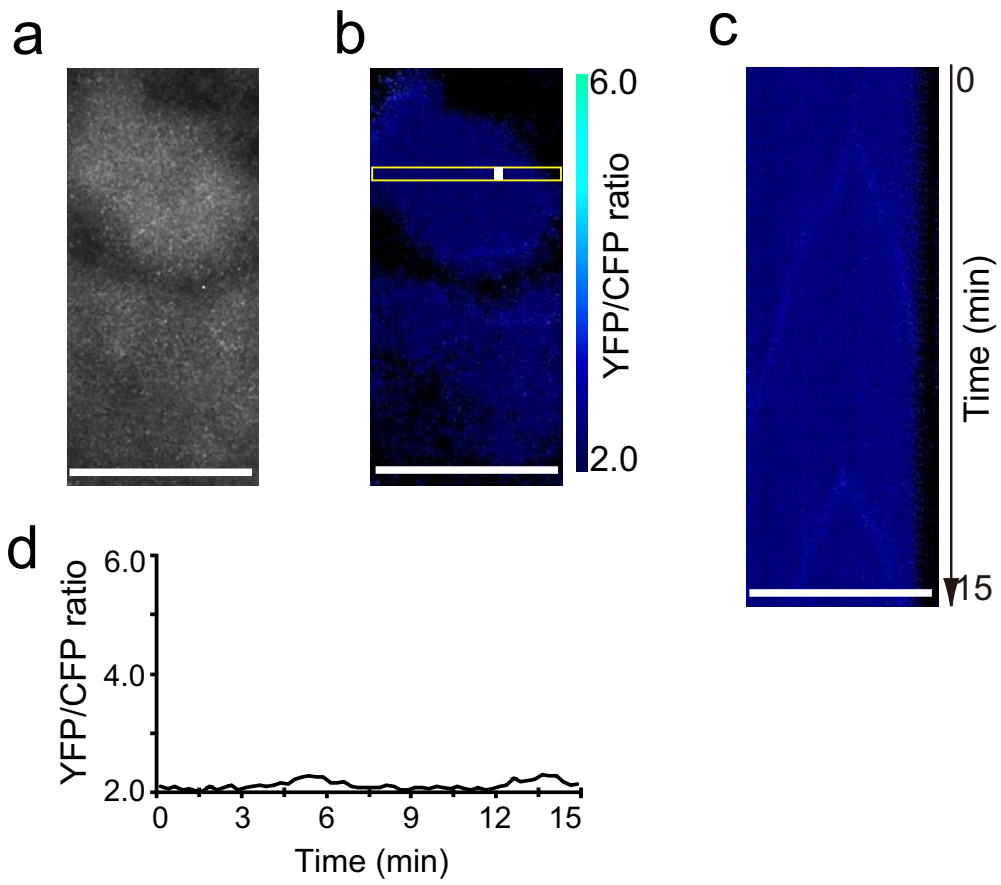

Supplementary Figure 7| YC3.60 and YC-Nano15 signals in response to trains of action potentials. (**a**) Maximum fluorescence intensity projection of a YC-Nano15-expressing pyramidal neuron, and expanded single z-section images within the white boxes. Bar, 5 μm. Line-scan images along the red line in response to 20 action potentials evoked at 20 Hz (arrowhead, stimulus onset). (**b**) Responses of YC3.60 (black) and YC-Nano15 (red) in layer 2/3 cortical pyramidal neurons to 1, 2, 5, and 10 action potentials evoked at 20 Hz (bar; stimulus period). $\Delta R/R_0$ traces averaged from 3 trials are shown.(**c**) Single action potential response detected with YC-Nano15 in samples from P17 and P72 mice. $\Delta R/R_0$ traces averaged from 3 trials are shown. Bar or arrow, stimulus timing.

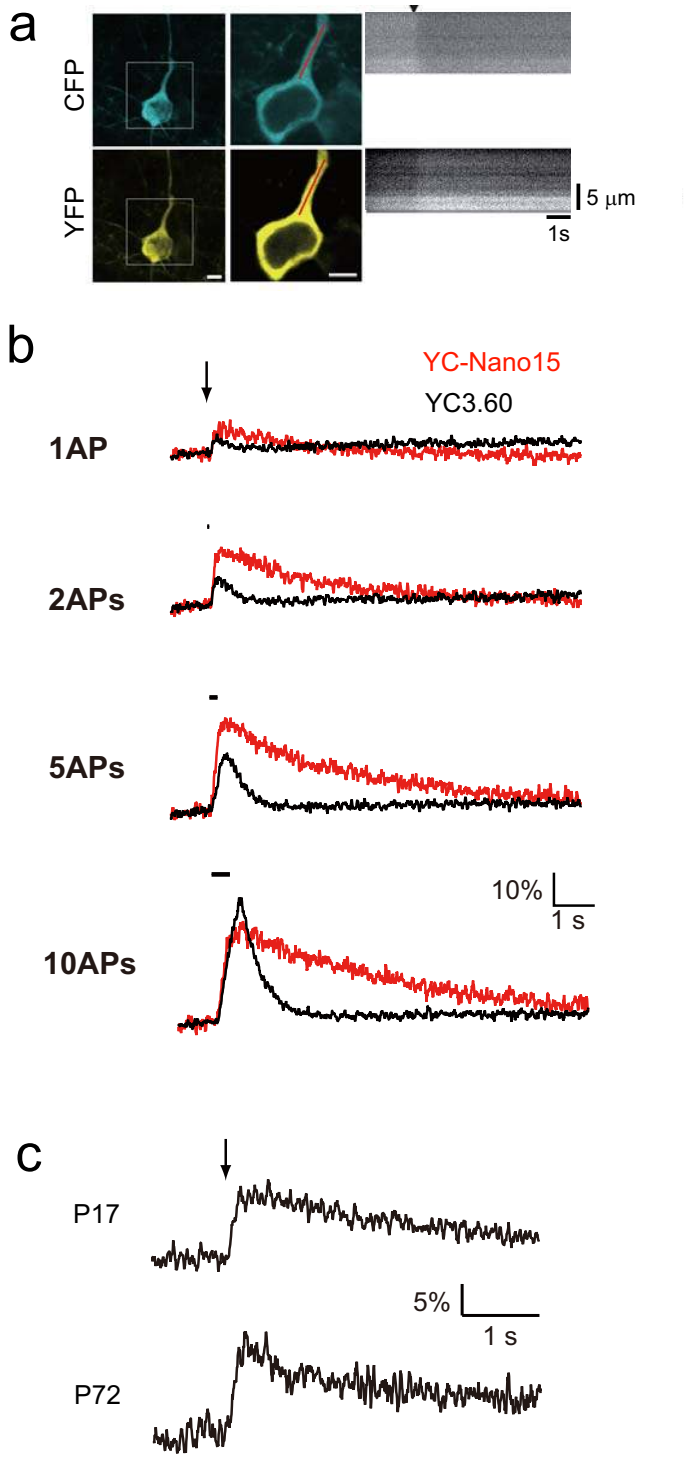

Supplementary Table 1 | Properties of new YC variants

	Dynamic range, %	R_{max}	R_{min}	K'_d, nM	Hill coefficient	Fraction, %
YC3.60	1,400	30	2	215.0	3.6	33
				779.6	**1.2**	**67**
YC-Nano140	1,300	28	2	**140.5**	**2.0**	**62**
(YC3.60 3GS)				754.1	0.9	38
YC2.60	1,300	28	2	**93.5**	**2.7**	**80**
				950.3	1.0	20
YC-Nano65	1,300	28	2	**64.8**	**1.6**	**90**
(YC3.60 4GS)				1441.3	1.8	10
YC-Nano50	1,250	27	2	**52.5**	**2.5**	**82**
(YC2.60 2GS)				403.8	1.0	18
YC-Nano30	1,250	27	2	**31.2**	**2.4**	**83**
(YC2.60 3GS)				204.8	1.3	17
YC-Nano15	1,450	31	2	**15.8**	**3.1**	**72**
(YC2.60 4GS)				320.2	0.6	28

Supplementary Table 2 | Electrophysiological properties of layer 2/3 pyramidal neurons expressing calcium sensors. All values are corrected for liquid junction potential (12 mV). There was no significant difference among the values from YCnano15-expressing cells, YC3.60-expressing cells and control cells (one-way ANOVA). [a] resting membrane potential. [b] input resistance. [c] threshold voltage for action potential generation. [d] amplitude of action potential measured from resting membrane potential. [e] half width of action potential.

Electrophysiological property		YCnano15 (n=14)	YC3.60 (n=7)	WT (n=5)	p-value
V_m [a]	(mV)	-81.4±6.5	-85.9±3.2	-81.2±11	0.33
R_m [b]	(MΩ)	209±59	-195±54	156±54	0.23
AP threshold[c]	(mV)	-46.2±5.4	-44.9±4.5	-42.9±6.9	0.51
AP amplitude[d]	(mV)	100±6.8	95.4±12	105±20	0.41
AP half width[e]	(ms)	2.46±0.58	3.69±2.3	1.97±0.68	0.063

Supplementary Note 1

Biochemical properties of YCs

In the present paper, we report different values for the dynamic range of Ca^{2+} detected from the values we reported previously (560%)[12] for YC2.60 and YC3.60, as well as different K_ds for Ca^{2+}. We attribute the difference to the greater purity of the recombinant proteins examined in this study. Here, to determine the dynamic range of the signal change in the indicators precisely, polyhistidine and biotin analog tags were attached to the YC proteins' N- and C-termini, respectively, and the proteins were sequentially purified by a Ni-NTA column and StrepTactin beads column, thereby only purifying the full-length recombinant proteins. On the other hand, the single-step purification with the Ni-NTA column used in the previous report resulted in a small amount of contamination with irregularly digested proteins, which interfered with the dynamic-range measurement.

After obtaining the highly purified YCs, we further determined the FRET efficiency of the YC-Nano. We calculated it to be 43% in the absence of Ca^{2+} and 93% in the presence of saturating Ca^{2+}, by the following equation:

$E = 1 - F_{DA}/F_D$ (eq. 1)

where E is the FRET efficiency, and F_{DA} and F_D are the fluorescence intensity of the donor in the presence and absence of the acceptor, respectively. F_D was obtained by measuring the fluorescence intensity of the YC-Nano after digestion with proteinase K (**Supplementary Fig 3**). Trypsin digestion gave an almost identical value for the FRET efficiency (data not shown).

Supplementary Note 2

Kinetics analysis

To understand how the elongated linker affected the kinetic properties, we measured the Ca^{2+}-association kinetics by stopped-flow photometry. Due to the feasibility of controlling the Ca^{2+} concentration above the 100 nM range, we measured the tau for the Ca^{2+} association reaction from zero Ca^{2+} to various Ca^{2+} concentrations for YC3.60 and YC3.60 modified with the elongated linker (3GS) (+4; Gly-Gly-Gly-Ser). By fitting the observed data to the equation, $k_{obs} = k_{on} [Ca^{2+}] + k_{off}$, we obtained comparable dissociation rate constants for YC3.60 and YC-Nano140 (0.34 and 0.33 s^{-1}, respectively), and an increased rate constant for the on reaction for YC-Nano140 (1.33×10^6 $M^{-1}s^{-1}$ for YC3.60 and 2.36×10^6 $M^{-1}s^{-1}$ for YC-Nano140). These data nicely account for the increased Ca^{2+} affinity of the molecule containing the elongated linker, because the apparent dissociation constant (K_d) calculated from the following equation $K_d = k_{off} / k_{on}$, where we obtained K_ds for YC3.60 and YC-Nano140 of 255 nM and 139 nM respectively, were comparable to the values obtained by the independent Ca^{2+} titration experiment (high-affinity fraction K_d = 215 and 140 nM for YC3.60 and YC-Nano140, respectively (see **Supplementary Table 1**). These results suggest that linker elongation accelerates the Ca^{2+}-induced conformational change of CaM-M13, which might be sterically restricted by the shorter linker.

Although we would like to measure the k_{off} of YC2.60 and its high affinity variants such as YC-Nano15, we could not do it because it was very difficult to precisely control free Ca^{2+} concentration at around few tens of nM as far as we used EGTA (K_d for Ca^{2+} = 151 nM in 0.1 M ionic strength, pH 7.2 at 25 ºC). For this purpose,

much stronger Ca^{2+} chelator with a smaller K_d value was required. However there is no such Ca^{2+} chelator available now. Therefore it was almost impossible to experimentally determine the k_{on} and k_{off} values of YC2.60 and its high affinity variants. Because YC3.60 have an affinity-lowering mutation, E104Q, in the CaM moiety, it would be reasonable to assume that k_{off} of YC2.60 and its variants were much smaller than that of YC3.60, while their k_{on}s were comparable. The slow decay kinetics of YC-Nano15 in neurons (**Fig. 2**, **Supplementary Fig. 7**, see **Supplementary Note 3**) could be explained by the smaller k_{off} of YC-Nano15 than that of YC3.60.

Supplementary Note 3

Combined electrophysiology and two-photon imaging.

To verify the properties of the high-affinity YCs in living neurons, we generated recombinant adenoviruses carrying YC-Nano15 and YC3.60 cDNA. The YCs were introduced into mouse brain by the high titer adenoviral vectors on embryonic day 14, which expressed as described in Methods section. At 15-72 postnatal days (P15-P72), an acute slice was prepared and subjected to a combination of electrophysiology and two-photon imaging. Electrophysiological properties of patched layer 2/3 pyramidal neurons are as follows; a resting potential of –85.9 ± 3.2 mV (YC3.60, n = 7), –81.4 ± 6.5 mV (YC-Nano15, n = 14) and -81.2 ± 11 mV (control, n = 5), an input resistance of 195 ± 54 MΩ (YC3.60, n = 7), 209 ± 59 MΩ (YC-Nano15, n = 14) and 156 ± 54 MΩ (control, n = 5), and a threshold for action potential generation of –44.9 ± 4.5 mV (YC3.60, n = 7), –46.2 ± 5.4 mV (YC-Nano15, n = 14) and –42.9 ± 6.9 mV (control, n = 5), suggesting that the YC-Nano15 as well as YC3.60 do not cause specific side effects at the expression level achieved by the CAG promoter (**Supplementary Table 2**). Current pulses were injected into the soma of whole-cell-patched layer 2/3 pyramidal neurons, and the fluorescence intensity change was line-scanned at the apical dendrite (**Supplementary Fig. 7a**). To correlate the number of AP and FRET signal changes, a series of current-triggered trains of 1, 2, 5, or 10 action potentials were elicited at a frequency of 20 Hz. The averaged $\Delta R_{YC3.60}$ (P15 mice, n = 5) was 5.5 ± 1.2 for the single action potential, 9.0 ± 1.5 for two, 20.6 ± 6.8 for five, and 41.4 ± 12.9 for ten action potentials **(Fig. 2a)**. That of YC-Nano15 (ΔR_{Nano15} at P17 or P19, n = 7) was 10.4 ± 1.9 for the single, 16.3 ± 3.7 for two, 26.4 ± 7.7 for five, and 31.8 ± 11.6 for ten APs

(Fig. 2a). The SNR for 1, 2, 5, and 10 APs was 2.9, 4.6, 10.1, and 21.0 for YC3.60, and 4.2, 5.9, 9.5, and 11.4 for YC-Nano15, indicating that YC-Nano15 has a higher detection sensitivity for the subtle Ca^{2+} transients associated with a single or small number of APs.

As expected, YC-Nano15 is not suitable for the detection of the large Ca^{2+} transients triggered by high-frequency stimulus, due to the signal saturation and the slow decay time (3-4 sec) (more than 10 APs at 20 Hz or trains of single APs at 2 Hz **Fig. 2b**). It would be reasonable to use YC-Nanos for the detection of non-bursting Ca^{2+} spikes of less than 1 Hz, similar to D3cpV, which possesses similar properties, including the single-AP sensitivity, saturating frequency, and slow decay time[4].

The single-AP sensitivity of YC-Nano15 was also verified in neurons subjected to long-term expression. The ability of YC-Nano15 to detect a single AP response was not affected in the cortical neurons from an acute slice of P72 mice (n = 3, **Supplementary Fig. 7c**), suggesting that the long-term expression of high-affinity YC is not very toxic under our experimental conditions.

Supplementary Note 4

Toxicity of YC-Nano in short-term expression.

To examine the short-term effect of YC-Nano, we injected different amounts of the indicators into zebrafish embryos, and checked the embryos' viability (**Fig A**, n > 90 for each experimental condition). Their viability was not severely affected at the low expression level (less than 10 μM at 24 hpf), where ratiometric imaging can be easily achieved. Less viability at higher loading level (more than 10 μM) was evident in Venus-loaded embryos suggesting non-specific effect of protein injection. However, the toxic effect in YC-Nano50 and YC3.60 might be partially resulted from interference of the CaM-M13 peptide domains with endogenous signaling pathways as reported elsewhere[4, 6].

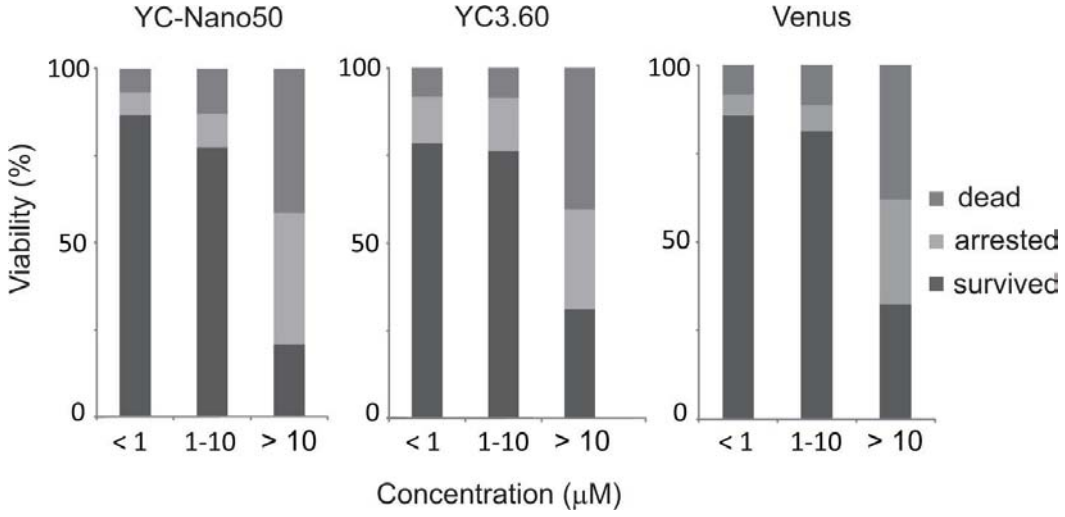

Fig. A. Viability of zebrafish embryos injected with different amounts of YCs.

Supplementary Note 5

Confocal imaging of the twitching behavior in zebrafish embryos.

At 17 hours post fertilization (hpf), zebrafish embryos initiated a spontaneous twitching behavior[24] that persisted until 30 hpf with decreasing frequency from 1 to 0.1 Hz (**Supplementary Video 4**). We found that YC-Nano50 was the best indicator to detect cellular activity in these living fish embryos. Cells loaded with high-affinity YC (Nano15) showed small donor signals compared with acceptor signals, which is not ideal for FRET measurement. This was partially because of cross-excitation of the YFP with the 458-nm laser line that is commonly used in confocal microscopes, and partially due to the large FRET signals, reflecting the relatively high Ca^{2+} levels, especially in a subset of cells (neurons) under resting conditions. On the other hand, cells loaded with low-affinity YC (YC3.60) showed donor signals in neurons (estimated to have a high Ca^{2+} level), but the FRET change was small due to the sub-optimal Ca^{2+} affinity (**Fig. 3**).

For confocal observation of the Ca^{2+} transients during the spontaneous twitching behavior, purified YC-Nano50 protein was injected into fertilized eggs (approx. final concentration of 5 μM), and the Ca^{2+} transients in the spinal neurons and muscles were imaged simultaneously by a widely used confocal microscopy method. We detected bilaterally alternating firing of a subset of spinal cord neurons (**Fig. 3** and **Supplementary Video 4**). Simultaneous with the neuronal firing, we also detected [Ca^{2+}] increases in the fast and smooth muscle. These results clearly revealed the spatio-temporal firing pattern of the cellular network involved in the spontaneous twitching behavior of a living animal. We also found that our high-affinity indicator

revealed different FRET signals depending on the cell type: high FRET signals for the epidermis and spinal neurons, and low FRET signals for fast and smooth muscles, suggesting different basal [Ca^{2+}] levels in living embryos. These results strongly support the idea that optimization of the indicator's properties, for the organism, the cell type, and the context of the stimulation, is essential for successful live-cell imaging.

References

24. Saint-Amant, L., & Drapeau, P., *J. Neurobiol*. **37**(4) 622-632 (1998)